Quantum mechanical treatment of the F+H2→HF+H reaction

Michael Baer, Julius Jellinek, and D. J. Kouri

Citation: The Journal of Chemical Physics **78**, 2962 (1983); doi: 10.1063/1.445257
View online: http://dx.doi.org/10.1063/1.445257
View Table of Contents: http://scitation.aip.org/content/aip/journal/jcp/78/6?ver=pdfcov
Published by the AIP Publishing

Quantum mechanical treatment of the $F+H_2 \rightarrow HF+H$ reaction

Michael Baer[a)b)]

Soreq Nuclear Research Center, Yavne, Israel 70600
and Department of Chemical Physics, Weizmann Institute of Science, Rehovot, Israel 76100

Julius Jellinek[b)]

Department of Chemical Physics, Weizmann Institute of Science, Rehovot, Israel 76100

Donald J. Kouri[a)]

Departments of Chemistry and Physics, University of Houston—Central Campus, Houston, Texas 77004
(Received 13 October 1981; accepted 7 July 1982)

In this paper is presented a quantum dynamical study of the $F + H_2$ reaction within the infinite order sudden approximation for the energy range $E_{tot} = 0.28$–0.50 eV. Results at various stages of the calculation are given ranging from the most detailed phases and S matrices to the total integral cross sections. The accuracy of the IOS is assessed by comparisons of the average l-labeled quantal IOS results with exact classical, initial-l labeled classical IOS, and l-initial labeled quantum IOS results. Comparison with experiment indicates that the qualitative state-to-state angular distributions are reproduced within this method. On the other hand, vibrational branching ratios for the product HF molecule are only partially reproduced. The main part of the discussion in the paper is devoted to the recent hypothesis concerning the existence of a superposition of resonances which strongly influence the angular distributions as a function of final vibrational state of the HF product.

I. INTRODUCTION

Recently, the infinite order sudden approximation has been introduced for reactive scattering (RIOS).[1–3] It was first applied to the $H + H_2$ system, for which it was found to yield very encouraging results.[2,4–9] This was achieved in spite of the fact that the calculations were carried out for very low energies where the nonreactive IOS is known, from other studies, not to be highly accurate and for a very unfavorable mass combination (i.e., three light atoms). The application of the RIOS was recently extended to the $F + H_2 \rightarrow HF + H$ reaction.[10] This extension is not straightforward. The $F + H_2$ system, in contrast to $H + H_2$, is not symmetric and so many unresolved difficulties which could be circumvented in the $H + H_2$ case due to symmetry could not be ignored in the more general $F + H_2$ case. These difficulties and their resolution will be discussed to a certain extent in the theory section of this paper (Sec. II).

The $F + H_2$ system is one of the most important systems within the field of chemical physics and has probably been studied more, both experimentally and theoretically, than any other atom-diatom reactive system. The main reason for the overwhelming interest in this reaction is that it is the major reaction in the most powerful gas laser available.[11–13] This fact has attracted an extensive experimental effort, which has ranged from the determination of absolute and relative rate constants[14–17] to the chemiluminescence and laser studies to determine product vibrational and rotational state distributions[18–22] and the application of molecular beam techniques to determine state-to-state differential cross sections.[23] The existence of this wealth of experimental data has in turn stimulated a large number of theoretical studies which can essentially be divided into two categories. First are structural studies which are aimed at obtaining the potential surface which governs the motion of the atoms during the reaction[24–36]; second have been dynamics studies which range from statistical models through classical trajectory studies and finally quantum mechanical scattering studies.[25–29,36–52]

Most recently, Sparks *et al.*[23] have carried out measurements of state-to-state angular distributions which are now being analyzed to yield the state-to-state differential cross sections. These data should provide much new information needed to construct the correct potential surface. The electronic structure and dynamical studies which have been carried out so far have already yielded much information about the surface. However, up to now, a completely satisfactory surface has not been obtained and those which looked most promising could not be examined completely because until very recently no quantum mechanical (QM) method was available to carry out quantum dynamics. Recently, however, such methods have been developed[53–55] and among them, as already mentioned earlier, is the RIOS.[1–3] The aim of this paper is to show that the dynamics performed within this version of the RIOS[1] yield results in qualitative agreement with the recent experiments of Sparks *et al.*[23]

The principal results of this study are (i) the qualitative sideways shift of the $v_f = 2$ HF product angular distribution is obtained, (ii) evidence for reso-

a)These authors were supported in part under grants from the Energy Laboratory, University of Houston—Central Campus and in part under a grant from the National Science Foundation.

b)These authors were supported in part under a grant from the US–Israel Binational Science Foundation.

 0021-9606/83/062962-16$2.10

nance effects in the $v_f=2$ product are found, (iii) resonance tuning arising from the γ dependence of the potential and from the centrifugal potential is proposed as the explanation of the sideways shift in the $v_f=2$ HF product angular distribution, (iv) the tuning effect is present over a range of energies so that the resonance effects are most likely not confined to a narrow range around the energy at which Sparks *et al.*[23] observed sideways peaking of the $v_f=2$ HF product, (v) the effective broadening of the resonance effects due to tuning by γ and l may prevent the usual resonance signature of a bump in the energy dependence of the total cross section from being observed, (vi) the relative vibrational state populations appear to show strong quantum effects.

II. THEORY

The theory of the RIOS was introduced in detail in Ref. 1 and additional comments, modifications and clarifications were given in Ref. 7. Although in both of these papers we considered for the most part a general (nonsymmetric) reaction still the fact that the theory was tested with respect to the fully symmetric $H+H_2$ system limited the discussion to certain aspects of this approximation. In the present section, we shall summarize again the main formulas for obtaining the differential and the integral reactive cross sections emphasizing the modifications introduced with respect to the previous formulation. Also, we reiterate for the sake of completeness, the main formulas needed to do the matching and while doing so introduce a few alterations associated with more general asymmetric reactions.

A. Differential and integral cross sections

The degeneracy averaged differential cross section from a given initial state $(v_\lambda j_\lambda m_\lambda)$ to a final vibrational state v_ν and all rotational states is given by[2]

$$\frac{d\sigma(v_\nu|v_\lambda j_\lambda m_\lambda|\theta,\psi)}{d\omega}=\frac{1}{(2j_\lambda+1)}\sum_{j_\nu m_\nu}|f(v_\nu j_\nu m_\nu|v_\lambda j_\lambda m_\lambda|\theta,\psi)|^2 , \tag{1}$$

where λ and ν denote the initial and final arrangements, ω is a solid angle comprised of the scattering angle θ, and the azimuthal angle ψ; v_α, j_α and $m_\alpha, \alpha=\lambda,\ \nu$ are the vibrational, rotational and the p helicity quantum numbers, respectively, and $f(v_\nu, j_\nu m_\nu|v_\lambda, j_\lambda m_\lambda|\theta,\psi)$ is the scattering amplitude function. In what follows, we drop the v_λ and v_ν indices to simplify the notation.

The differential scattering amplitude is related to the body-fixed matrix element according to

$$f(j_\nu m_\nu|j_\lambda m_\lambda|\theta,\psi)=\frac{i^{j_\lambda-j_\nu+1}}{2k_{j_\lambda}}\sum_J[J]d^J_{m_\lambda m_\nu}(\theta)S^{j_\nu m_\nu}_{Jj_\lambda m_\lambda} , \tag{2}$$

where $[x]$ stands for $(2x+1)$ and $d^J_{m_\lambda m_\nu}(\theta)$ is the Wigner rotation matrix (the notion of Rose[56] is employed). The body fixed S matrix elements are related to the Arthurs–Dalgarno (AD)[57] matrix elements by

$$S^{j_\nu m_\nu}_{Jj_\lambda m_\lambda}=\sum_{l_\nu l_\lambda} i^{l_\lambda-l_\nu}\frac{\sqrt{[l_\lambda][l_\nu]}}{[J]} \times\langle l_\lambda 0 j_\lambda m_\lambda|Jm_\lambda\rangle\langle l_\nu 0 j_\nu m_\nu|Jm_\nu\rangle S^{j_\nu l_\nu}_{Jj_\lambda l_\lambda} \tag{3}$$

and the AD S matrix elements are approximated within the RIOS as[7]

$$S^{j_\nu l_\nu}_{Jj_\lambda l_\lambda}=i^{l_\lambda+l_\nu-2\bar{l}}\sum_{\Omega_\lambda\Omega_\nu}\frac{\sqrt{[l_\nu][l_\lambda]}}{[J]}\langle l_\lambda 0 j_\lambda\Omega_\lambda|J\Omega_\lambda\rangle\langle l_\nu 0 j_\nu\Omega_\nu|J\Omega_\nu\rangle ,$$

$$2\pi\int_0^\pi d\gamma_\lambda\sin\gamma_\lambda y^*_{j_\nu\Omega_\nu}[\gamma_\nu(B,\gamma_\lambda),0] \times d^J_{\Omega_\lambda\Omega_\nu}[\Delta(\gamma_\lambda,B)]S_{\bar{l}}(\gamma_\lambda)y_{j_\lambda\Omega_\lambda}(\gamma_\lambda,0) , \tag{4}$$

where $\gamma_\alpha,\ \alpha=\lambda,\nu$ is defined as

$$\gamma_\alpha=\cos^{-1}(\hat{r}_\alpha,\hat{R}_\alpha)\ ;\ \ \alpha=\lambda,\nu \tag{5}$$

and Δ is an angle defined as

$$\Delta=\cos^{-1}(\hat{R}_\lambda,\hat{R}_\nu) . \tag{6}$$

B is a parameter which originates from the matching of the λ channel wave function with the ν channel wave function (more details about B will be given in the next section) and $\bar{l}$ is the CS orbital parameter[58,59] which is identified either as the initial value of the angular momentum quantum number in the λ arrangement channel, namely l_λ, or as the average value; i.e.,

$$\bar{l}=(l_\lambda+l_\nu)/2 . \tag{7}$$

In the first case the l labeling[58,59] is known as the l-initial labeling[58] and in the second as the l-average labeling.[59] In the integral we have also a collinear-type γ dependent (and also B and $\bar{l}$ dependent) S matrix element. We will elaborate more about this function in the next section. Equation (4) differs from the previous formula given in Eq. (115) in Ref. 1 by the fact that here the variable of integration is γ_λ, whereas there it was γ_ν.

In the theoretical study of KKB[1] it was assumed that γ_ν is the independent variable and γ_λ is the dependent one and consequently the final integration in Eq. (115) of Ref. 1 was carried out with respect to γ_ν. However, this is not correct and the detailed derivation of Eq. (4) will be given in a later paper. At this point, we simply note that a careful examination of the approach of KKB leads to Eq. (4) with γ_λ as the integration variable.

Before considering the important question of matching in the general asymmetric reaction case, we also wish to discuss briefly the result obtained earlier for the l-initial degeneracy averaged differential cross section, summed over all final rotational states. In Ref. 7, this quantity was obtained subject to the restriction that the matching surface parameter B was equal to one. In fact, the result obtained is completely general for any value of B and $\bar{l}=l$ initial,[58] and the details of the derivation follow exactly parallel to those given in Ref. 7. The final result is

$$\frac{d\sigma}{d\omega}(v_\nu|v_\lambda j_\lambda m_\lambda|\theta\psi)=\frac{1}{8(k^\lambda_{v_\lambda j_\lambda})^2}\sum_{\substack{l_\lambda l'_\lambda\\ L}}[l_\lambda][l'_\lambda]d^L_{00}(\theta)\langle l_\lambda 0 l'_\lambda 0|L0\rangle^2 ,$$

$$\int_0^\pi d\gamma_\lambda\sin\gamma_\lambda S^{\nu v_\nu}_{\lambda v_\lambda l_\lambda}(\gamma_\lambda)S^{\nu v_\nu}_{\lambda v_\lambda l'_\lambda}(\gamma_\lambda)d^L_{00}[\Delta(\gamma_\lambda,B)] , \tag{8}$$

which is valid for any B value.

B. The determination of the $S_l(\gamma_\lambda)$ matrix element

The numerical treatment within the rotational IOS, whether being quantum mechanical or classical, is essentially a fixed angle [(γ) fixed] "collinear-type" treatment. In the nonreactive case, only one angle has to be considered as only one arrangement channel is encountered. In the reactive case where at least two arrangement channels are involved, at least two angles have to be considered at a time; an angle γ_λ and an angle γ_ν (in what follows we consider the case of two arrangement channels only). The two angles may or may not be dependent on each other. So far, we assumed in all our quantum mechanical RIOS treatments γ_ν to be uniquely determined once γ_λ has been assigned a value (recently Jellinek and Baer[60-63] developed a classical mechanical RIOS and also considered the possibility of treating γ_λ and γ_ν as two independent variables).

To begin with, we assume that γ_λ and γ_ν are two independent angles. The three coordinates $(r_\lambda, R_\lambda, \gamma_\lambda)$ describe a three-mathematical-dimensional space in which γ_λ is a polar coordinate. Fixing γ_λ reduces the three-dimensional geometry to a plane. The same three-dimensional geometry space can be described in terms of the three coordinates $(r_\nu, R_\nu, \gamma_\nu)$ and again, assigning γ_ν a fixed value reduces the three-dimensional space to a plane (the two planes are different). Since, in general, two planes can only intersect along a single straight line the same happens here and this line is the line we previously termed the *matching line* or the *border line*. In Ref. 60 we were able to prove that the equation of this line is uniquely determined by the relation

$$r_\nu = B r_\lambda \ , \tag{9}$$

where B is a well defined function of γ_λ and γ_ν, i.e.,

$$B = B(\gamma_\lambda, \gamma_\nu) \ . \tag{10}$$

To summarize, fixing γ_λ and γ_ν reduces the three-dimensional space to two planes that intersect along a straight line which goes through the region. The next step is to consider the corresponding Schrödinger equation which will describe the motion of the three particles on the two intersecting planes. Extension of the nonreactive case leads to

$$-\frac{\hbar^2}{2\mu}\left\{\left[\frac{1}{R_\alpha^2}\frac{\partial}{\partial R_\alpha}R_\alpha^2\frac{\partial}{\partial R_\alpha}+\frac{1}{r_\alpha^2}\frac{\partial}{\partial r_\alpha}\left(r_\alpha^2\frac{\partial}{\partial r_\alpha}\right)-\frac{\bar{l}_\alpha(\bar{l}_\alpha+1)}{R_\alpha^2}\right.\right.$$
$$\left.\left.-\frac{\bar{j}_\alpha(\bar{j}_\alpha+1)}{r_\alpha^2}\right]+V(R_\alpha, r_\alpha, \gamma_\alpha)-E\right\}\psi_\alpha = 0 \ ; \quad \alpha = \lambda, \nu \ , \tag{11}$$

where $\bar{l}_\alpha$ and $\bar{j}_\alpha$ $\alpha = \lambda, \nu$ are the IOS parameters[58,59] mentioned before, E is the total energy (we assume conservation of total energy and consequently we have the same total energy on both planes), R_α and r_α $\alpha = \lambda, \nu$ are the translational and vibrational *mass scaled* coordinates, and μ is the symmetric mass[53]

$$\mu = \left(\frac{m_\lambda m_\nu m_k}{m_\lambda + m_\nu + m_k}\right)^{1/2} \ . \tag{12}$$

In order to solve Eq. (11) we perform the substitution

$$\psi_\alpha = \frac{1}{R_\alpha r_\alpha} G_\alpha \ ; \quad \alpha = \lambda, \nu \ , \tag{13}$$

which leads to

$$-\frac{\hbar^2}{2\mu}\left\{\left[\frac{\partial^2}{\partial R_\alpha^2}+\frac{\partial^2}{\partial r_\alpha^2}-\frac{\bar{l}_\alpha(\bar{l}_\alpha+1)}{R_\alpha^2}-\frac{\bar{j}_\alpha(\bar{j}_\alpha+1)}{r_\alpha^2}\right]\right.$$
$$\left.+V(R_\alpha, r_\alpha, \gamma_\alpha)-E\right\}G_\alpha = 0 \ ; \quad \alpha = \lambda, \nu \ . \tag{14}$$

In order to have a unique solution for the wave function on each plane as well as along the matching line, the following conditions, along the *border* line, are imposed:

$$G_\lambda = G_\nu \ , \tag{15}$$

$$\nabla_\lambda G_\lambda = -\nabla_\nu G_\nu \ , \tag{16}$$

where ∇_α stands for the two-dimensional *grad* operation:

$$\nabla_\alpha = \hat{R}_\alpha \frac{\partial}{\partial R_\alpha} + \hat{R}_\alpha \frac{\partial}{\partial r_\alpha} \ ; \quad \alpha = \lambda, \nu \ . \tag{17}$$

It should be emphasized that our recent $H + H_2$ results[4,6-8] were derived employing a somewhat different kind of matching. However, comparing these results with those obtained applying the above, it was found that the results were the same to within a few percent.

Once the wave function is fully determined its asymptotic form can be analyzed and the corresponding S matrix can be obtained. In general, these S-matrix elements depend on six parameters (except for the energy), namely $\bar{l}_\alpha$, $\bar{j}_\alpha$, and γ_α, $\alpha = \lambda, \nu$. In all the calculations reported, it was assumed that $\bar{j}_\lambda = \bar{j}_\nu = 0$ and that $\bar{l}_\lambda = \bar{l}_\nu = \bar{l}$. As for the two angles γ_λ and γ_ν, instead of having both independent, only γ_λ was assumed to be free, with γ_ν then being uniquely determined by fixing B. It has been shown that in this case the equation for $\cos\gamma_\nu$ is[1]

$$\cos\gamma_\nu = -\frac{[\cot\gamma_\lambda + (1-B^2)\cot\phi_{\lambda 0}\cot\alpha]}{B[1+(1-B^2)\cot^2\phi_{\lambda 0}]^{1/2}} \ , \tag{18}$$

where

$$\cot\phi_{\lambda 0} = \frac{\sin\alpha}{B^2 - \cos^2\alpha} \times (\cos\alpha\cos\gamma_\lambda + \sqrt{B^2 - \sin^2\gamma\cos^2\alpha}\,) \tag{19}$$

and

$$\cos\alpha = -\left(\frac{m_\lambda m_\nu}{(m_\lambda + m_k)(m_\nu + m_k)}\right)^{1/2} \ , \tag{20}$$

$$\sin\alpha = +\sqrt{1-\cos^2\alpha} \ . \tag{21}$$

In the present calculation we assumed B to equal 1.4, a value which yields a matching line that follows very closely the potential dividing line in the plateau region for most configurations. Although B might be considered as a parameter it is believed that the "primitive" fixed γ_λ-S matrix elements $S_l(\gamma_\lambda)$, as well as the final fixed-body S matrix elements are only weakly dependent on B as long as the reaction is collinearly dominated. In this connection it should be mentioned that recently Jellinek and Baer (JB)[61,62] obtained classical RIOS cross sections for the same system by performing classical trajectory calculations on the above fixed γ_λ and γ_ν planes. The calculations were performed for two different values of B; i.e., $B = 1.0$ and 1.4. The results for the integral total cross sections were identical although there were some changes observed with regard to the final vibrational distributions (in particular the

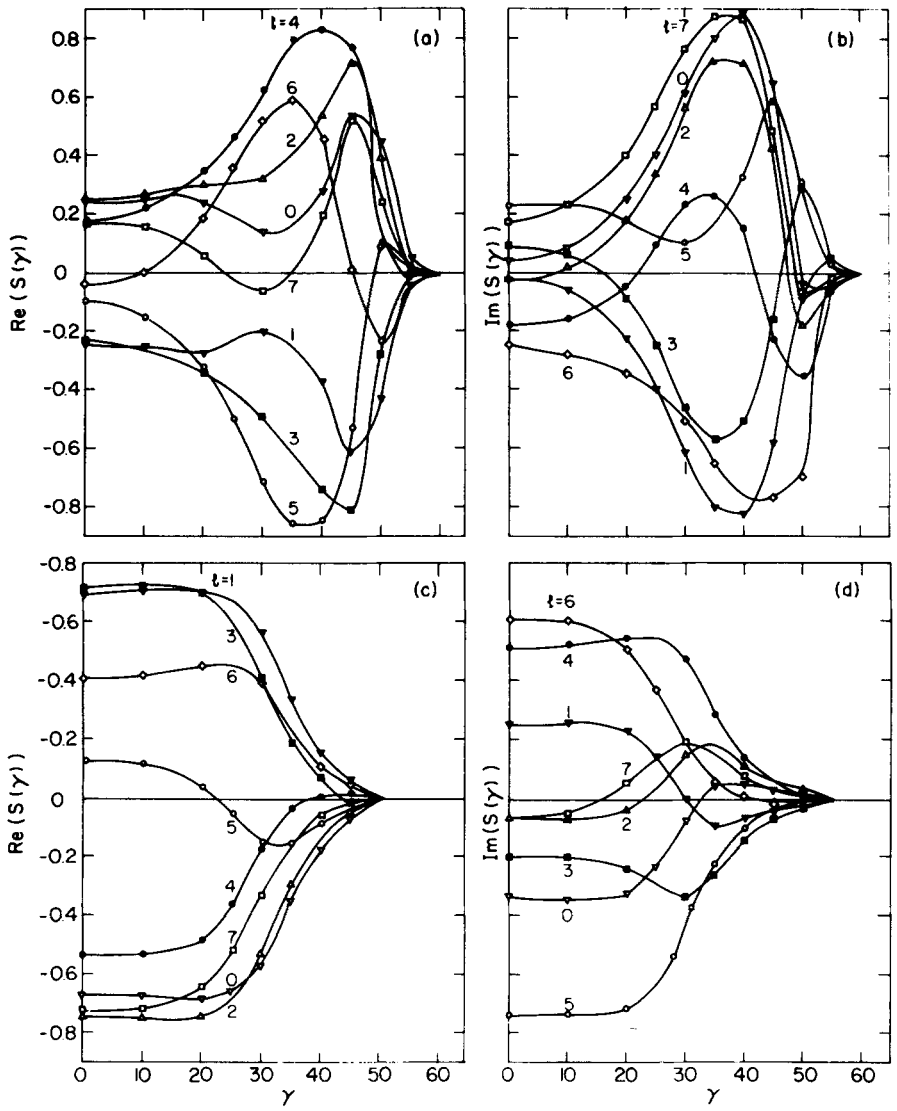

FIG. 1. Primitive $S_l(v_i=0 \rightarrow v_f)$ matrix elements (real and imaginary) as a function of γ_λ for various low l values and $E_{tot}=0.423$ eV. (a) Re$[S(v_i=0 \rightarrow v_f=2)]$; (b) Im$[S(v_i=0 \rightarrow v_f=2)]$; (c) Re $[S(v_i=0 \rightarrow v_f=3)]$; (d) Im$[S(v_i=0 \rightarrow v_f=3)]$.

branching ratios $\sigma(v_i=0; v_f=3)/\sigma(v_i=0; v_f=2)$ changed from 0.6 to about 1.0). It is felt that these classical RIOS results strongly support our belief that the precise value of B does not strongly influence the results obtained.

C. Factorization of the RIOS for general B value

In Ref. 7 we also derived a factorization relation within the l initial RIOS which expresses a general reactive amplitude for $\lambda v_\lambda j_\lambda m_\lambda \rightarrow \nu v_\nu j_\nu m_\nu$ in terms of that for the $j_\lambda = m_\lambda = 0$ initial rotational states. The derivation was carried out, however, again with $B=1$. The derivation for a general value of B is completely analogous to that for $B=1$, and the result is

$$S^{\nu v_\nu j_\nu \Omega_\nu}_{J \lambda v_\lambda j_\lambda \Omega_\lambda} = \sum_{\substack{l \Omega'_\lambda \\ j'_\nu \Omega'_\nu}} [l] \begin{pmatrix} l & j_\lambda & J \\ 0 & \Omega'_\lambda & -\Omega'_\lambda \end{pmatrix} \begin{pmatrix} l & j_\lambda & J \\ 0 & \Omega_\lambda & -\Omega_\lambda \end{pmatrix}$$

$$\times \left[2\sqrt{\pi} \int_0^\pi y^*_{j_\nu \Omega_\nu}[\gamma_\nu(\gamma_\lambda, B), 0] d^J_{\Omega_\nu \Omega'_\lambda}(\Delta) y_{j_\lambda \Omega'_\lambda}(\gamma_\lambda, 0) \right.$$

$$\left. \times d^l_{\Omega'_\nu 0}(\Delta) y_{j'_\nu \Omega'_\nu}[\gamma_\nu(\gamma_\lambda, B), 0] \sin\gamma_\lambda d\gamma_\lambda \right] S^{\nu v_\nu j'_\nu \Omega'_\nu}_{l \lambda v_\lambda 00} . \quad (22)$$

This result states that, just as for the nonreactive IOS,[58] the general reactive amplitudes are completely determined by that out of the $j_\lambda = m_\lambda = 0$ initial rotational state. However, because of the more complicated spectroscopic coefficient (compared to the nonreactive case[58]), the cross section for a general reactive transition does not simply scale in terms of the reactive cross sections out of the $j_\lambda = m_\lambda = 0$ initial state. There arise additional interference terms. However, when these are small, one will also expect to see scaling at the cross section level for the l-initial RIOS.

III. RESULTS

We shall present three types of results; namely the primitive (angle dependent) S matrix, and probability results, angle averaged probabilities and opacity functions and finally the differential and integral cross sections. In what follows all the results discussed are for $v_i=0$ and $j_i=0$.

A. Primitive results: γ-dependent S-matrix elements, phases, and probabilities

In Fig. 1 are shown the reactive primitive $S_l(\gamma)$ matrix elements as a function of γ for $E=0.423$ for dif-

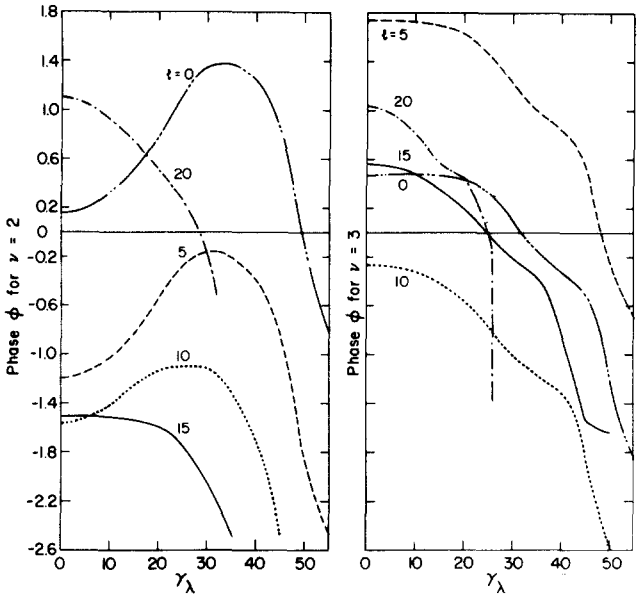

FIG. 2. Primitive phases $\phi(v_i = 0 \rightarrow v_f)$ as a function of γ_λ for various l values and for $E_{tot} = 0.423$ eV. (a) The phase of $v_f = 2$; (b) The phase for $v_f = 3$.

ferent l values. In Figs. 1(a) and 1(b) are given the results for $v_f = 2$ and in Figs. 1(c) and 1(d) for $v_f = 3$. We display separately the real part of $S_l(\gamma)$ [cf. Figs. 1(a) and 1(c)] and the imaginary part [cf. Figs. 1(b) and 1(d)]. As can be readily seen the figures for $v_f = 2$ are very different from those for $v_f = 3$. The curves 1(c) and 1(d) are relatively smooth, with hardly any wiggles. The curves for various l values slowly decay to zero as γ changes from $\gamma = 0$ to $\gamma \simeq 50°$. On the other hand, the results for $v_f = 2$ given in Figs. 1(a) and 1(b) show much more structure, and the curves tend to oscillate and peak primarily at angles in the range $30° \leq \gamma \leq 40°$. We shall see momentarily the significance of the different behavior between the $v_f = 2$ and $v_f = 3$ results. The results shown so far are for a single energy which is in the vicinity of what has been conjectured to be a resonant energy.[23,47] However, we note that in general similar patterns were observed for energies both below and above this energy. In Fig. 2 are presented some phases of the $S_l(\gamma)$ matrix elements as a function of γ for different l values. In Fig. 2(a) are shown the $v_f = 2$ phases and in Fig. 2(b) the $v_f = 3$ phases. In the case of the phases, we again see a qualitative difference between the phases for $v_f = 2$ and $v_f = 3$. The phase for $v_f = 2$ has a nonmonotonic variation with γ while that for $v_f = 3$ decays from a maximum at $\gamma = 0$. We can understand the information contained in Figs. 1 and 2 much more easily if instead we use Argand plots. These are plots of $\mathrm{Re}[S_{if}(p)]$ versus $\mathrm{Im}[S_{if}(p)]$, where i and f represent some initial and final states and p is a parameter which increases monotonically. In our case the energy (as well as the orbital quantum number $\bar{l}$) is held fixed and the angle γ is used as a parameter (justification for this is discussed in the next section). Three plots of $S_l(v_i = 0 \rightarrow v_f = 2)$ for $l = 6$, 7, 8, and $E = 0.423$ eV are given in Fig. 3(a) where γ is the parameter which is changed monotonically from $\gamma = 0$ to $\gamma = 55°$, an angle for which the reaction probability is negligibly small. We recall that the complex number $S_l(\gamma)$ can be represented in terms of its modulus (the distance from the origin of the Argand plot to the point of interest) and a phase ϕ (the same phase as plotted in Fig. 2). Because for each value of l the $S_l(\gamma)$ makes a loop in the complex plane, the phase ϕ must first increase with increasing γ and then decrease as γ continues to increase to its maximum value at 55°. At that point, the phase ϕ becomes ill de-

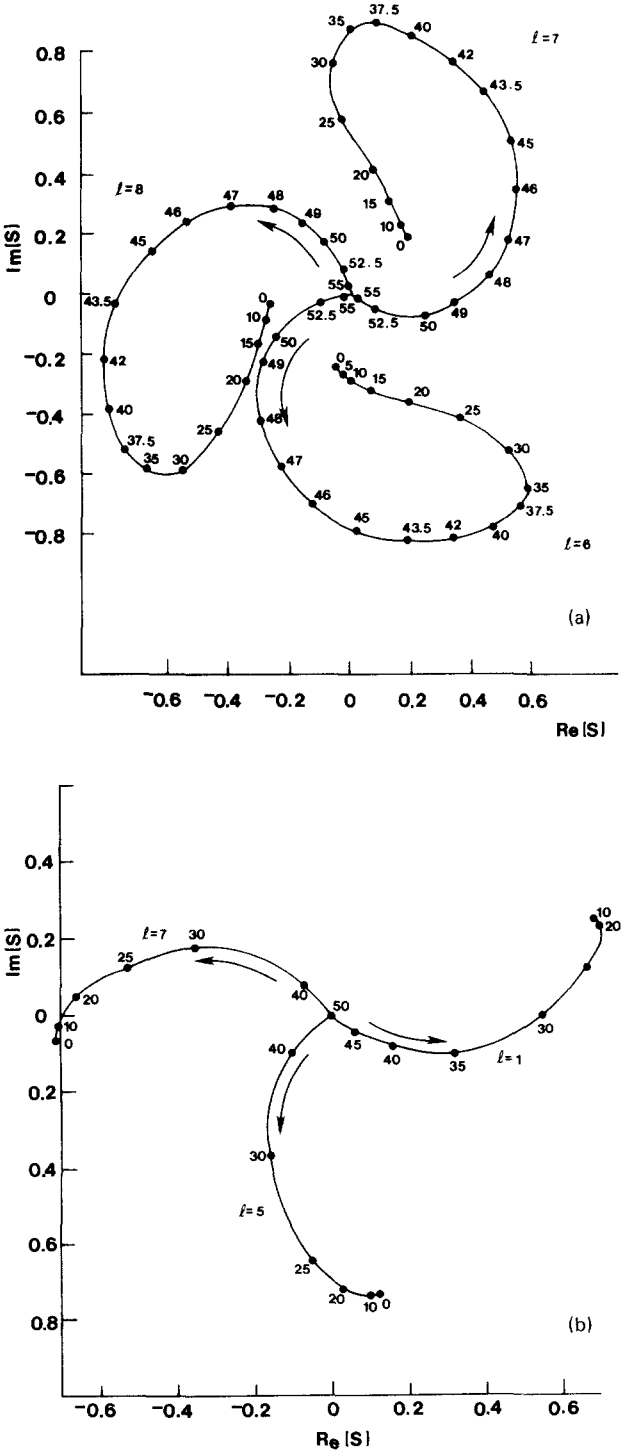

FIG. 3. Argand plots of $S_l(\gamma)$ with γ as the independent parameter and $E_{tot} = 0.423$ eV. Numbers stand for values of γ in degrees. (a) $v_f = 2$ and $l = 6$, 7, 8; (b) $v_f = 3$ and $l = 1$, 5, 7.

fined because the S matrix becomes essentially zero. Reference to Fig. 2 shows that this is precisely the behavior of ϕ for $v_f = 2$. In addition, we see in Fig. 3(a) that the loop structure of the Argand plots imply that the real and imaginary parts of $S_l(\gamma)$ will wiggle. For example, for $l = 7$ in Fig. 3(a), the ReS first decreases until it is negative and reaches a minimum, then increases to a maximum and then decreases to zero as γ ranges from 0° to 55°. Reference to Fig. 1(a) shows that this is exactly the oscillatory structure of ReS for $l = 7$ and $v_f = 2$. Thus, Fig. 3(a) is a compact summary of the results and allows us to understand them more easily. Now we recall that for structureless particle scattering, the occurrence of a counterclockwise (with increasing energy) perfect circle about the origin indicates the existence of a resonance. That is, it is indicative of a positive delay time and further, since in that case, $S = \exp(2i\phi)$, a complete loop about the origin implies an increase in phase by π radians. In the case of reactive (or nonreactive) scattering, the occurrence of a resonance no longer implies that the Argand plot show a counterclockwise perfect circle about the origin as energy is increased. This is easily seen when we recall that for structureless particles the perfect circle of unit radius arises simply because $|S|^2 = 1$ for all energies. In the reactive case, the probability can *never* equal one (due to the optical theorem). Furthermore, the modulus of the reactive S-matrix element must change as energy changes so that one does not expect a perfect circle of *any* given radius. Finally, in the structureless particle case, the counterclockwise circle always is about the origin since in that case, the S matrix can never vanish (again due to conservation of flux). For reactive scattering, this is no longer true. Thus, if there is a resonance in reactive scattering, the Argand plot need not yield a closed loop about the origin. This in turn implies that the phase ϕ for a reactive scattering resonance need not increase by π but in general will show a smaller increase. In the present case, we emphasize that our Argand plots are with respect to the parameter γ rather than energy. However, as γ increases in the strong interaction region, the effective energy available for translation decreases. Thus, high γ values effectively correspond to low kinetic energy and low γ values to high kinetic energies. It is then clear that in Fig. 3(a), the loops are *all* counterclockwise when one goes from low energy (high γ) to high energy (low γ) values. Thus, the results in Fig. 3(a) indicate a positive time delay. As to whether it should be termed a resonance, this depends in part on how large a range of energy must be traversed in order to complete the loop. In the present case, the loop is substantially complete when one goes from 55° to about 25° suggesting that there is a significant time delay.

In Fig. 3(b) we give Argand plots for $v_f = 3$ and several l values. In this case, it is easy to see the more or less monotonic decrease in phase ϕ as γ goes from 0° to 55°, just as was seen in Fig. 2. Also, the nonoscillatory behavior of the $S_l(\gamma)$ is readily seen (e.g., for $l = 7$, the ReS steadily increases as γ ranges from 0° to 55°. ImS, on the other hand, shows a single maximum). We also see that although the paths are all counterclockwise, the increase in phase which occurs is *much* smaller than for $v_f = 2$. Thus, it is clear that there is no resonance enhancement of $v_f = 3$.

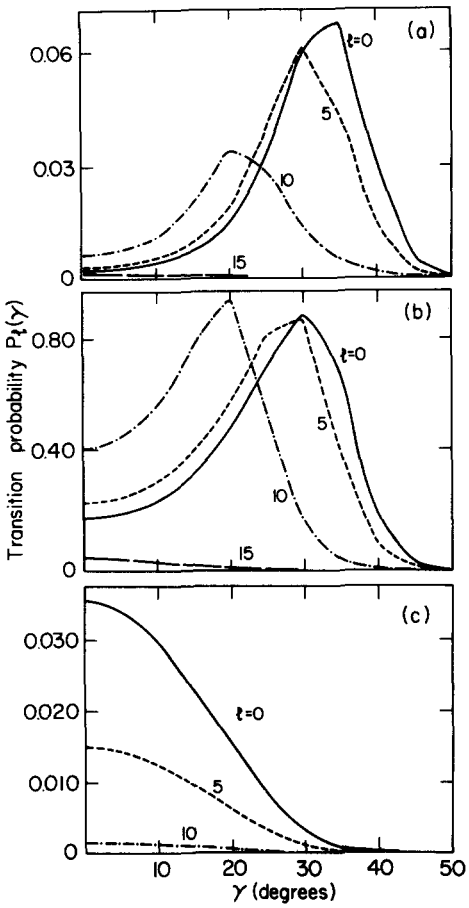

FIG. 4. Primitive reactive state-to-state probabilities $P(v_i = 0 \rightarrow v_f)$ as a function of γ_λ for different l values and for $E_{tot} = 0.34$ eV. (a) $P(v_i = 0 \rightarrow v_f = 1)$; (b) $P(v_i = 0 \rightarrow v_f = 2)$; (c) $P(v_i = 0, v_f = 3)$.

In Figs. 4 and 5 are shown reactive state-to-state probabilities as a function of γ for different l values. In Figs. 4(a) and 5(a) are shown the results for $v_f = 1$, in Figs. 4(b) and 5(b) for $v_f = 2$ and in Figs. 4(c) and 5(c) for $v_f = 3$. In Fig. 4 are shown the results for $E = 0.34$ eV and in Fig. 5 for $E = 0.423$ eV.

The main features to be noticed are: (a) the probabilities for $v_f = 1, 2$ and for $v_f = 3$ exhibit a different γ dependence for most of the l values. Probabilities for $v_f = 1$ and $v_f = 2$ tend to peak at angles which are far removed from the collinear arrangement while the $v_f = 3$ probabilities all have a maximum at $\gamma = 0$, and then slowly decay to zero as γ increases. (b) The differences between the results in Fig. 4 and in Fig. 5 are not essential in nature and both exhibit very similar patterns. The only noticeable changes are that all the probabilities, as a function of γ, extend to larger γ values when the energy is increased from $E = 0.34$ eV to $E = 0.423$ eV. Also the $v_f = 1, 2$ results tend to shift their peak region to higher angles. As for $v_f = 3$, most of the highest probabilities are still concentrated around the collinear arrangement.

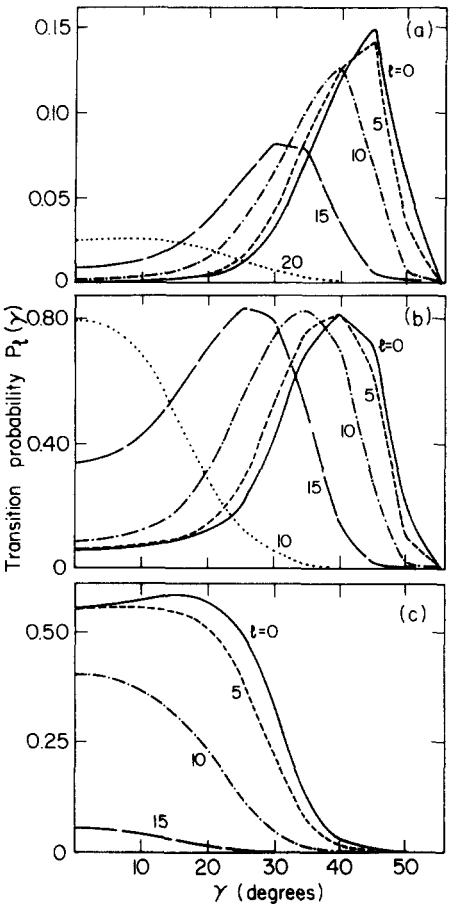

FIG. 5. Primitive reactive state-to-state probabilities $P(v_i = 0 \rightarrow v_f)$ as a function of γ_λ for different l values and for $E_{tot} = 0.423$ eV. (a) $P(v_i = 0 \rightarrow v_f = 1)$; (b) $P(v_i = 0 \rightarrow v_f = 2)$; (c) $P(v_i = 0, v_f = 3)$.

In Figs. 6 and 7 are shown probabilities as a function of l for different angles. In each figure are given three curves which correspond to $v_f = 1, 2, 3$. In Fig. 6 are presented the results for $E = 0.36$ eV and in Fig. 7 for $E = 0.423$ eV. It is noticed that the probabilities for $v_f = 1, 2$ peak at l values which are usually far removed from the value $l = 0$. The curves for $v_f = 3$, however, always attain their highest value at $l = 0$ and then monotonically decrease to zero as l increases.

Another feature to be noticed for the $v_f = 1, 2$ curves is that the more collinear the arrangement, the narrower the peak as a function of l. *The height of the peak for the $v_f = 2$ curves is essentially independent of γ.*

In Fig. 8 are shown reactive transition probabilities as a function of energy ($E = 0.28 - 0.7$ eV) for a few values of γ and l. The state-to-state $P(v_i = 0 \rightarrow v_f = 2)$ probabilities are shown in Figs. 8(a), 8(c), and 8(e), and the state-to-state $p(v_i = 0 \rightarrow v_f = 3)$ probabilities are shown in Figs. 8(b), 8(d), and 8(f). In each figure, three curves which correspond to three different l values are given. We first call attention to the clear presence of the $(l = 0, \gamma = 0)$ resonance at $E_{tot} \sim 0.28$ eV that was detected long ago.[41,42] This $(l = 0, \gamma = 0)$ resonance is characterized by a steep rise in probability followed by an equally steep fall to a shoulder, which would seem to be due to interference between the background and resonance scattering. This shoulder then descends more slowly to an even broader shoulder. For $\gamma = 0$, $v_f = 2$ [Fig. 8(a)], increasing l causes a significant broadening of the resonance peak which washes out the first shoulder that was seen in the $l = 0$, $\gamma = 0$ curve. However, the very broad second shoulder remains as a feature for all the $\gamma = 0$, $v_f = 2$ results.

By contrast, the $\gamma = 0$, $v_f = 3$ [Fig. 8(b)] results show the normal rise at threshold followed by a steady decline in the probability. *Because there is no resonance, one does not observe the shoulder which is so evident in the $v_f = 2$, $\gamma = 0$ results.* In Fig. 8(c) we have the results for $v_f = 2$, $\gamma = 30°$ and we observe that the $l = 0$ case is qualitatively like the $\gamma = 0$, $v_f = 2$, $l = 10$ or 20 cases in Fig. 8(a). One has the resonance peak which is again broadened and shifted to higher energy compared to the

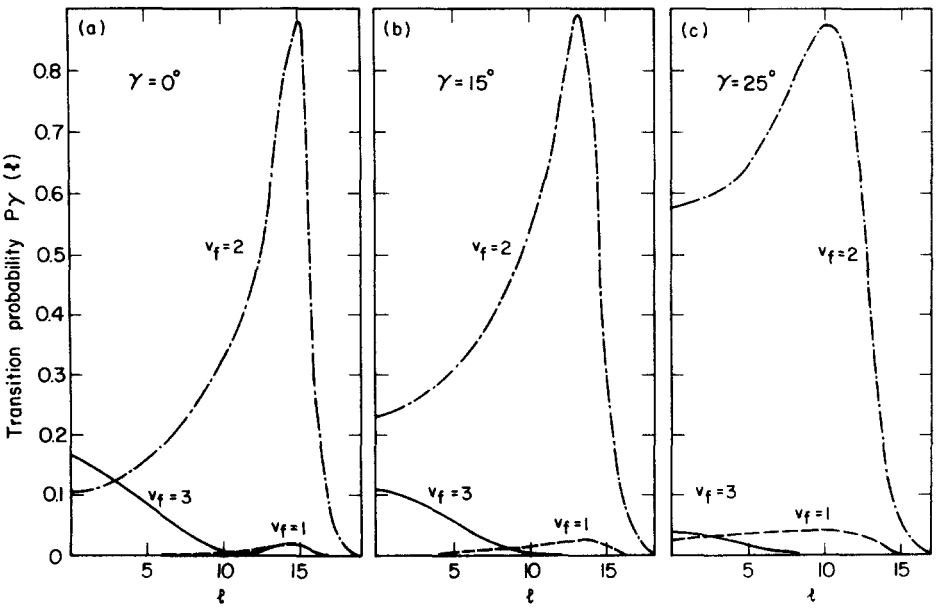

FIG. 6. Primitive reactive state-to-state probabilities $P(v_i = 0 \rightarrow v_f)$ as a function of l for different γ_λ values and for $E_{tot} = 0.36$ eV. (a) $\gamma_\lambda = 0°$; (b) $\gamma_\lambda = 15°$; (c) $\gamma_\lambda = 25°$.

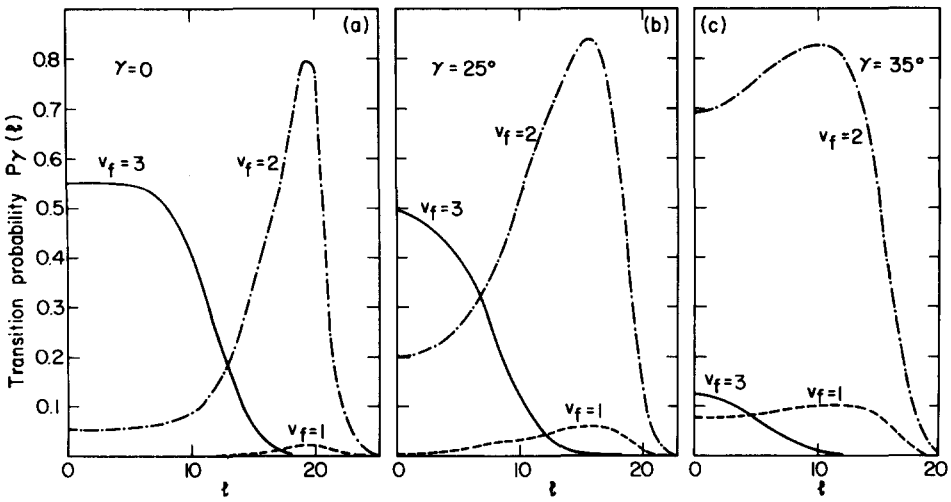

FIG. 7. Primitive reactive state-to-state probabilities $P(v_i=0 \rightarrow v_f)$ as a function of l for different γ_λ values and for $E_{tot}=0.423$ eV. (a) $\gamma_\lambda=0$; (b) $\gamma_\lambda=25°$; (c) $\gamma_\lambda=35°$.

$\gamma=0$, $l=0$, $v_f=2$ case. In fact, again for $l=10$ and 20, $\gamma=30°$, and $v_f=2$, one sees the broadened resonance peak followed by the shoulder produced by the background nonresonant reaction probability. The $v_f=3$, $\gamma=30°$ results again show no resonant peak followed by a nonresonant shoulder. Finally, when $\gamma=50°$, the $v_f=2$ results do not seem to show a resonance feature. Regarding the $(v_i=0 \rightarrow v_f=3)$ results, an important thing to note is the appearance of a resonance for the collinear arrangement and $l=0$ at the vicinity of $E_{tot}=0.7$ eV (see also Ref. 42). Another feature is the relatively high threshold energies as compared with those of the $(v_i=0 \rightarrow v_f=2)$ transitions once the angle γ becomes large.

B. Angle averaged results

In Fig. 9, are presented, for the three energies $E=0.36$, 0.423, and 0.50 eV respectively, the angle averaged probability functions $P_{v_f}(l)$ as a function of l. They were obtained from the primitive probability functions $P_{v_f}(l,\gamma)$ according to the expression

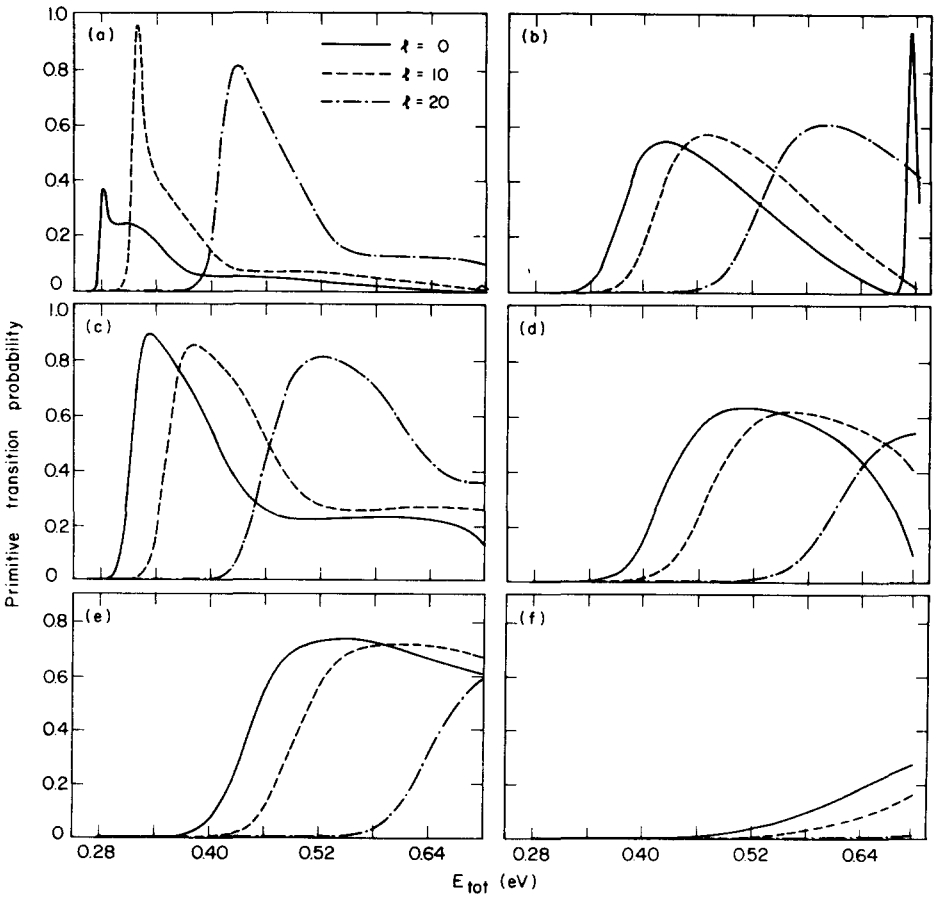

FIG. 8. Primitive reactive state-to-state probabilities $P(v_i=0 \rightarrow v_f)$ as a function of the energy for different γ_λ and l values: (a) $\gamma_\lambda=0°$, $v_f=2$; (b) $\gamma_\lambda=0°$, $v_f=3$; (c) $\gamma_\lambda=30°$, $v_f=2$; (d) $\gamma_\lambda=30°$, $v_f=3$; (e) $\gamma_\lambda=50°$, $v_f=2$; (f) $\gamma_\lambda=50°$, $v_f=3$.

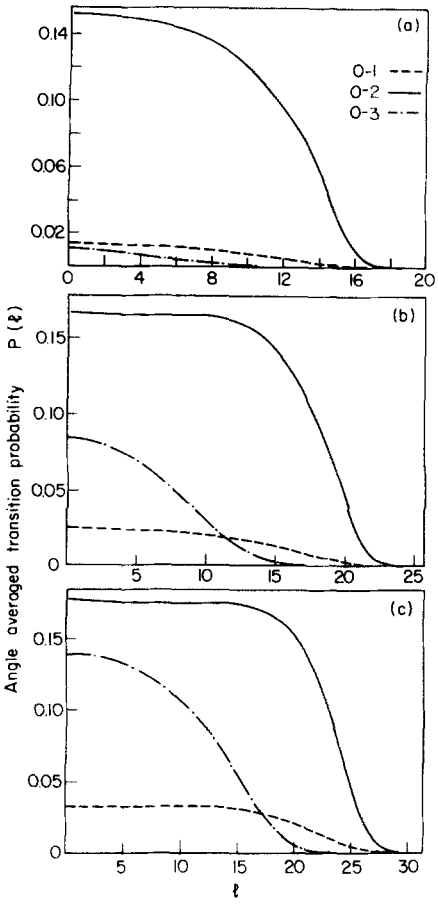

FIG. 9. Angle averaged reactive state-to-state probabilities as a function of l for different energies: (a) $E_{tot} = 0.36$ eV; (b) $E_{tot} = 0.423$ eV; (c) $E_{tot} = 0.50$ eV.

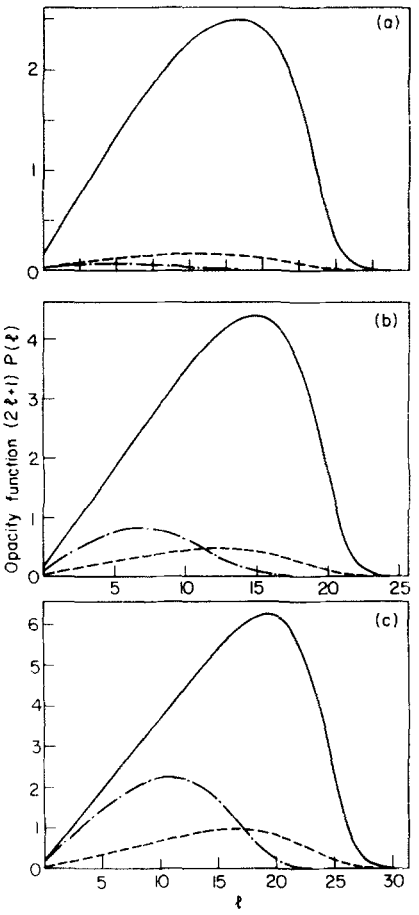

FIG. 10 Angle averaged state-to-state l-weighted probabilities as a function of l for different energies: (a) $E_{tot} = 0.36$ eV; (b) $E_{tot} = 0.423$ eV; (c) $E_{tot} = 0.50$ eV.

$$P_{v_f}(l) = \int_0^1 d(\cos\gamma) P_{v_f}(l,\gamma) \ . \tag{23}$$

In each figure are shown three curves giving the $v_f = 1$, 2, 3 probability functions. The main feature to be noted is the difference in shape between the $v_f = 1$, 2 curves and the $v_f = 3$ curve. The first two not only extend to larger l values, but also have a rectangular form. In contrast, the $v_f = 3$ curves extend to a shorter l range and decrease monotonically to zero.

In Fig. 10 are shown the corresponding l-weighted probabilities defined by

$$\bar{P}_{v_f}(l) = (2l+1) P_{v_f}(l) \ . \tag{24}$$

These results are also shown in order to get a better feeling for the relative significance of each $P_v(l)$. The multiplication of $P_{v_f}(l)$ by $(2l+1)$ causes each $\bar{P}_{v_f}(l)$ (including those for $v_f = 3$) to obtain their maximal value at an l value $[= \bar{l}_v(E)]$ different from zero. It is seen (as expected) that

$$\bar{l}_{v_f=2}(E) > \bar{l}_{v_f=1}(E) > \bar{l}_{v_f=3}(E) \ , \tag{25}$$

and that all $l_{v_f}(E)$ are monotonically increasing functions of E.

C. Differential and integral cross sections

In Figs. 11–15 are shown the state-to-state l-average reactive differential cross sections[64] (degeneracy averaged over m_λ, summed over m_v and j_v but resolved with respect to the final vibrational state v_v). In each figure, three curves are given for the reactive cross sections into $v_f = 1$, 2, and 3 at a given total energy. All the results are scaled to be equal to one at $\theta = \pi$, and display the following features:

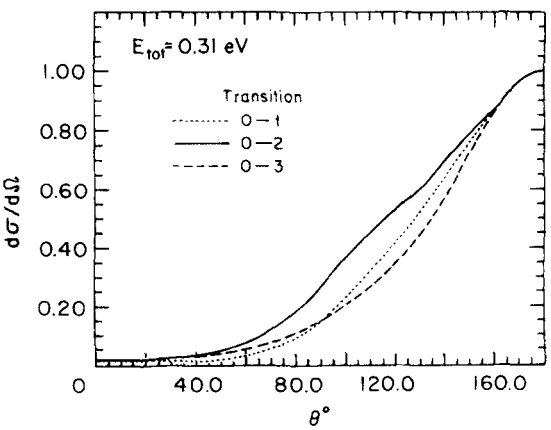

FIG. 11. Vibrational state resolved differential cross sections for incident energy $E_k = 0.043$ eV $= 0.99$ kcal/mol; $v_f = 1$, $v_f = 2$, $v_f = 3$. The cross sections are all normalized to one at $\theta = 180°$ (the ratios being $1 : 2 : 3 = 0.039 : 1 : 3.5 \times 10^{-4}$).

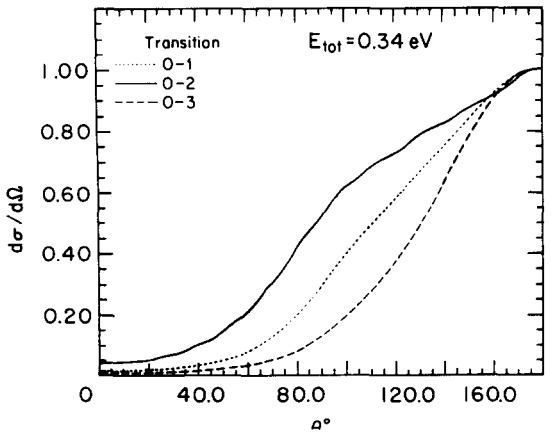

FIG. 12. Vibrational state resolved differential cross sections for incident energy $E_k = 0.073$ eV = 1.68 kcal/mol; $v_f = 1$, $v_f = 2$, $v_f = 3$. The cross sections are all normalized to one at $\theta = 180°$ (the ratios being 1 : 2 : 3 = 0.069 : 1 : 0.008).

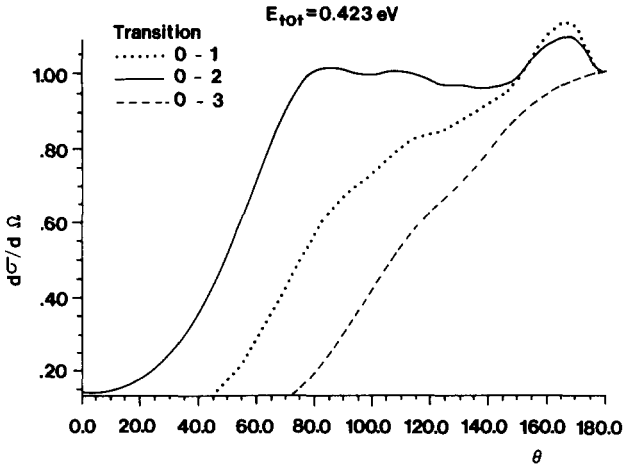

FIG. 14. Vibrational state resolved differential cross sections for incident energy $E_k = 0.156$ eV = 3.54 kcal/mol; $v_f = 1$, $v_f = 2$, $v_f = 3$. The cross sections are all normalized to one at $\theta = 180°$ (the ratios being 1 : 2 : 3 = 0.15 : 1 : 0.32).

(a) The differential cross section for $v_f = 3$ is backwards peaked at $\theta = \pi$ for all energies.

(b) The differential cross section for $v_f = 1$ is backwards peaked ($\theta \cong \pi$) for all energies studied but has a significant sideways component ($\theta \sim \pi/2$) at the highest energy.

(c) The differential cross section for $v_f = 2$ is backwards peaked ($\theta = \pi$) only for the three lowest energies; at the fourth it shows a secondary peak at $\theta \sim 100°$ and at the fifth it peaks at $\theta \sim \pi/3$.

(d) In addition, the differential cross section for $v_f = 2$ has oscillations, with the most pronounced occurring a little forward of π.

In the next section we discuss the relevance of these findings with respect to the experimental results.

In Fig. 16 are presented the total integral cross sections summed over all final vibrational states and in Figs. 17 and 18 are given the vibrational branching ratio ratios $\lambda(v_f, 2)$ defined as

$$\lambda(v_f, 2) = \frac{\sigma(v_i = 0 \rightarrow v_f)}{\sigma(v_i = 0 \rightarrow v_f = 2)} \tag{26}$$

for $v_f = 1, 3$, respectively.

In Fig. 16 are given five curves of which three summarize quantum mechanical (QM) results and two classical (CL) results. As for the QM curves, one is due to Redmon and Wyatt (RW)[47] and the other two are due to the present RIOS treatment. One RIOS result is an l-av calculation and the second is an l-in calculation. We note that due to increased accuracy the results for the l-av curve have been changed since our previous publications.[10,61] As for the classical curves, the first is from an exact classical trajectory calculation[40] and the second is from a classical RIOS treatment.[61] The following features are to be noted:

(a) The l-in RIOS and RW[47] quantal results are significantly smaller than the exact classical results.[40]

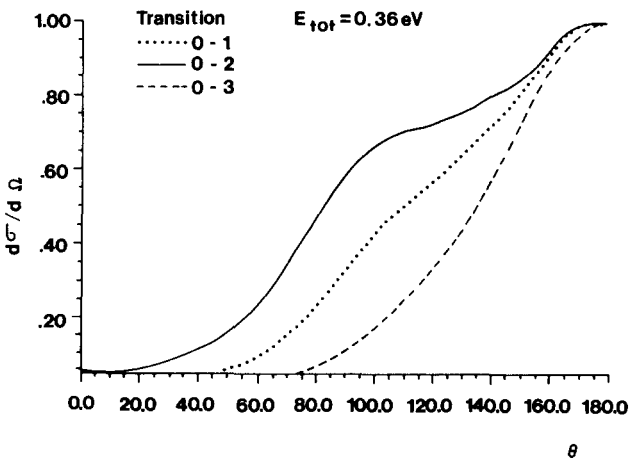

FIG. 13. Vibrational state resolved differential cross sections for incident energy $E_k = 0.093$ eV = 2.14 kcal/mol $v_f = 1$, $v_f = 2$, $v_f = 3$. The cross sections are all normalized to one at $\theta = 180°$ (the ratios being 1 : 2 : 3 = 0.093 : 1 : 0.035).

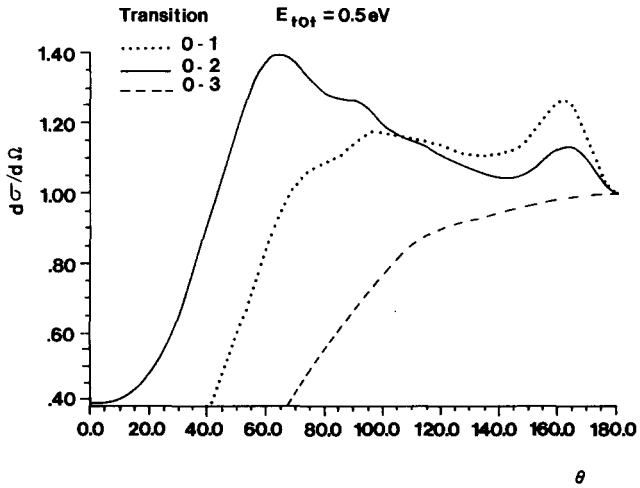

FIG. 15. Vibrational state resolved differential cross sections for incident energy $E_k = 0.233$ eV = 5.37 kcal/mol $v_f = 1$, $v_f = 2$, $v_f = 3$. The cross sections are all normalized to one at $\theta = 180°$ (the ratios being 1 : 2 : 3 = 0.19 : 1 : 0.59).

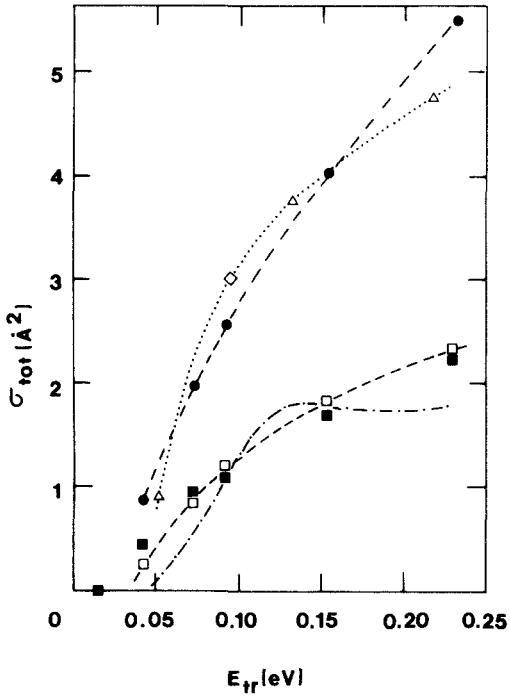

FIG. 16. Total integral cross sections for the reaction $F + H_2$ $(v_i = 0,\ j_i = 0) \rightarrow HF + H$ as a function of translation energy: △, ◇. Exact classical results (see Refs. 38 and 40); ● quantum mechanical l-av IOSA results; ■ quantum mechanical l-in IOS results; □ classical (l-in) IOS results; -•-•- quantum mechanical coupled states results (Ref. 47).

(b) The two l-in IOS treatments (the CL and the QM) yield, for all practical purposes, the same results which differ only in the very low energy region where tunneling effects are important.

(c) The l-av RIOS quantal results and the exact classical results are in rather good agreement.

The implications of these results will be analyzed in the next section.

In Figs. 17 and 18 are given two QM and two CL curves (it should be emphasized that the branching ratios for the QM l-in and the QM l-av are identical). The QM curves are those of RW and our present treatment and the CL curves are from the exact classical trajectory calculations[40] and from the CL RIOS treatment.

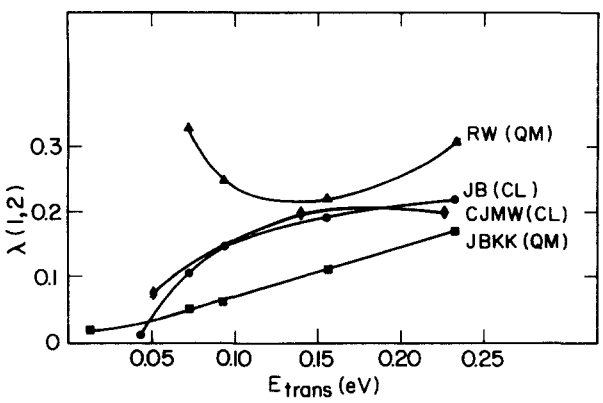

FIG. 17. Vibrational branching ratio $\lambda(1,2) = \sigma(v_i = 0 \rightarrow v_f = 1)/\sigma(v_i = 0 \rightarrow v_f = 2)$ as a function of translation energy. Quantum mechanical IOS results (squares), classical IOS results (dots), exact classical results (Ref. 40) (diamonds), quantum mechanical CS results (Ref. 47) (triangles).

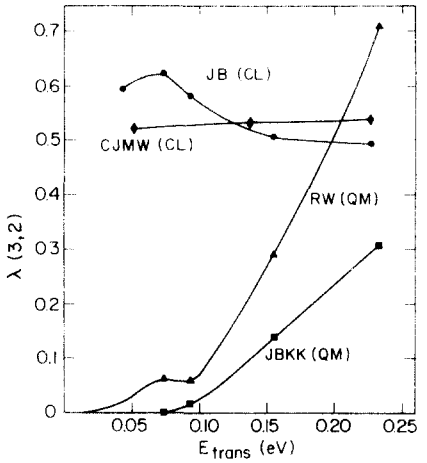

FIG. 18. Vibrational branching ratio $\lambda(3,2) = \sigma(v_i = 0 \rightarrow v_f = 3)/\sigma(v_i = 0 \rightarrow v_f = 2)$ as a function of translational energy. Quantum mechanical IOS results (squares), classical IOS results (dots), exact classical results (Ref. 40) (diamonds), quantum mechanical CS results (Ref. 47) (triangles).

The main features are:

(a) In Fig. 17 all branching ratios are relatively small. However, it is also to be noted that whereas the two classical results overlap very nicely, the two QM curves differ, particularly in the low energy region.

(b) Figure 18 emphasizes the major difference between the QM and the CL treatments. It is seen that the branching ratio $\lambda(3,2)$ is more or less flat in the two CL treatments, and the $v_f = 2$ product is not greatly favored over $v_f = 3$. By contrast, the QM results both show a strong energy dependence: in the low energy region the $v_f = 2$ is highly favored over the $v_f = 3$ state but as the energy increases their populations tend to become comparable.

IV. DISCUSSION

In the previous section we presented the basic results which we wish to discuss. We will concentrate on three aspects: (1) The accuracy of the RIOS results as compared to other treatments. (2) The importance of resonant phenomena and their influence on the numerical results. (3) Quantum effects in the $F + H_2$ system.

Although the second and the third subjects are closely related, we distinguish between the resonant and other quantum effects because of the considerable interest in the former.

A. The accuracy of the IOS results

It is difficult to analyze the accuracy of our QM–IOS results as there are no exact QM results available and the approximate CS results of RW were obtained using a modified version of the Muckerman V potential surface. Since, however, there are available exact CL

results, it would be desirable to formulate a classical reactive IOS and to test the IOS within the framework of classical mechanics. This has been recently done[60–62] and some of the results are shown in Figs. 16–18. It is to be noticed that whereas the total l-in classical IOS cross sections are smaller than the exact classical ones, the vibrational branching ratios are practically the same for the two CL methods. It is of interest to mention that recently Muckerman[36] indicated that at 3 kcal/mol ($\equiv 0.13$ eV) $\lambda(1,2)$ is equal to 0.24 and $\lambda(3,2)$ is equal to 0.5 which are again reasonably close to our CL IOS results. Unfortunately, the agreement, as far as the total cross sections are concerned, is not as good and the l-in CL IOS results are only about half as large as the exact CL ones. On the other hand, we notice that the l-in QM–IOS integral total cross sections are very close to the l-in CL–IOS cross sections but the branching ratios differ.

Next, we note that the l-av QM–IOS integral total cross section is in very good agreement with the exact classical result. Furthermore, the branching ratios for the l-av and l-in QM–IOS results are essentially identical.

These facts lead us to the following conclusions:

(a) On the basis that the l-in QM and CL IOS integral total cross sections agree very well with each other but are well below exact classical results, we conclude that the l-in version of the IOS does not give quantitative magnitudes for the integral total cross sections. However, the results do suggest that the integral total cross section does not contain large quantum effects. Thus, the exact classical results for the integral total cross section are probably close to the result one would obtain from a CC calculation.

(b) As was also observed for the $H + H_2$ system,[4,6–8] the l-av QM IOS appears to give much more accurate integral total cross sections than the l-in version. This is seen from the fact that the l-av QM IOS results for this quantity are in good agreement with exact classical (which as argued above are probably close to the results which would be obtained in an exact CC calculation).

(c) The agreement of the l-av and l-in QM IOS branching ratios with each other, and the agreement of the l-in CL IOS and exact classical branching ratios leads us to believe that the QM IOS gives reliable relative cross sections with either the l-in or l-av versions. Furthermore, we believe that the classical branching ratios (both exact and l-in CL IOS) will not agree with exact QM for this MV potential surface. This is supported by the qualitative agreement of the l-av and l-in QM IOS branching ratios with those obtained by RW with their QM CS method (but with a modified MV surface).

B. Resonant effects in the three-dimensional system

Collinear studies done some seven years ago pointed out the existence of a well-resolved resonance in the threshold energy region.[41–43] This finding has since been confirmed several times [see Fig. 8(a)]. Some speculations were made with respect to the importance of such resonances and their effect on three-dimensional systems. However, it was only in 1979, when RW[47] completed their CS calculation for this system, that results were available indicating the presence of a resonance in a three-dimensional reaction. As can be seen from Fig. 16 their total cross-section levels off around the energy $E_{\text{trans}} = 0.13$ eV. This leveling off was interpreted as being due to the end of a resonance enhanced rate of increase, at energies below 0.13 eV translational energy in the total (as well as the $v_i = 0 \rightarrow v_f = 2$) cross section. The fact that the location of the resonance was shifted from around $E_{\text{trans}} \sim 0.01$ eV in the collinear case [see Fig. 8(a)] to higher E_{trans} was argued to be a result of three-dimensional effects.

Further discussion on the possible effect of such a resonance was given in a recent publication by Sparks *et al.*[23] They performed molecular beam experiments in which they measured the state-to-state differential cross sections and found the $v_f = 2$ differential cross sections to behave differently from the other two (i.e., $v_f = 1, 3$) differential cross sections. Whereas for a low energy measurement ($E_{\text{trans}} \sim 0.1$ eV) they found that all three angular distributions peaked backwards, at a higher energy (~ 0.15 eV) they noticed a dramatic change in the $v_f = 2$ angular distribution. The other two distributions remained backward peaked but the $v_f = 2$ peaked sideways ($\sim 120°$). This behavior was consistent with the difference in the partial wave reactive probabilities of RW[47] for the two energies $E \sim 2$ and 3 kcal/mol. That is, at low energy, RW found a monotonic decline with l of the reactive $v_f = 2$ probability while at $E \sim 3$ kcal/mol, they observed a maximum for $v_f = 2$ at $l = 10$. In Figs. 11–15 we have given our QM–IOS angular distributions for $v_f = 1$, 2, 3 and as can be seen, they qualitatively fit the experimental findings. In particular for the three energies below or equal to 2.14 kcal/mol all three angular distributions peak backwards but for $E_{\text{trans}} = 0.156$ eV, which corresponds to $E_{\text{trans}} = 3.54$ kcal/mol a change in the $v_f = 2$ distribution is noticed. In contrast to the two others, it shows a strong sideways component at about 80°. At the energy 0.5 eV, the sideways peaking is very evident.

Since we have available all the "primitive" IOS information, namely the corresponding l-, γ-, and E-dependent S matrix elements, we can examine this possibility in a rather straightforward manner.

If a given S-matrix element, say $S_{v_i v_f}(E)$, is assumed to be in the vicinity of a single nonoverlapping resonance at energy E_0, it can be expressed in the form[65] (the Breit–Wigner formula)

$$S_{v_i v_f} = \frac{\Gamma/2}{E - E_0 + i\Gamma/2}, \tag{27}$$

where Γ is the width of the resonance. The corresponding phase shift $\phi_{v_i v_f}(E)$ can be shown to be of the form

$$\phi_{v_i v_f}(E) = \tan^{-1}\left(\frac{\Gamma/2}{E - E_0}\right). \tag{28}$$

Plotting $\phi_{v_i v_f}(E)$ as a function of E one may expect $\phi_{v_i v_f}$ to change abruptly by a value of π as the energy changes from just below to just above E_0. However, the above expression applies to the eigenphase shifts in the gen-

eral case of inelastic or reactive scattering. As we discussed earlier, in general for reactive scattering, the phase of the reactive S-matrix element will not increase by a full π. Furthermore, due to the energy dependence of background nonresonant scattering, even the eigenphase shifts will not in general increase by a full amount π. The same type change in $\phi_{v_i v_f}(E)$ can also be obtained by fixing E and varying E_0 from above E to below it. This is done in the following way.

The location of the resonance energy E_0 for each primitive case should be dependent on l and γ (this should be the case if the resonance is supposed to "move" due to three-dimensional effects). Thus $\phi_{v_i v_f}$ can be written as

$$\phi_{v_i v_f}(E; l, \gamma) = \tan^{-1}\left(\frac{\Gamma(l,\gamma)/2}{E - E_0(l,\gamma)}\right) . \tag{29}$$

Assuming now that $\Gamma(l,\gamma)$ is only weakly dependent on l and/or γ, then a continuous variation of E_0 as well as of $\phi_{v_i v_f}$ results from changing l or γ, or both, through the range of interest. An abrupt change of $\phi_{v_i v_f}$ resulting from fixing E and l but varying γ would indicate the existence of a resonance. In Fig. 2 are shown a few representative phases as a function of γ, and as can be seen, in the main γ range of interest, no change in ϕ by a full π is observed (sometimes abrupt changes in ϕ appear towards the end of the range of interest of γ where the corresponding $|S|^2$ matrix elements are relatively small). However, more information is obtained from the Argand plots (Fig. 3) as a function of the angle γ, $E = 0.423$ eV and $l = 6$, 7, 8. As mentioned previously, the signature of a resonance in an Argand plot for the reactive S matrix will not in general be a counterclockwise circle about the origin with unit radius but rather a counterclockwise loop showing a reasonably rapid increase in phase with increasing energy. Furthermore, just as in Fig. 3(a), the counterclockwise loop will not in general be closed due to the background phase energy dependence. In the case of the $v_f = 2$ results, the background phase appears to also have a substantial energy variation. Thus, the results in Fig. 3(a) would appear to show the presence of a resonance for all three l values. *It is important, however, to realize that the resonant behavior shown in Fig.* 3(a) *is not confined to the energy range at which Sparks et al.*[23] *observed the sideways peaking of the* $HF(v_f = 2)$ *product.* It is also present at lower energies. Thus, for a fixed l value and at a lower energy E, the value of $E_0(l,\gamma)$ which produces resonance changes to a lower value of γ. Alternatively, for a fixed value of γ and lower E, the value of l for which resonance occurs is also lower. This feature is shown quite graphically in Figs. 4–7. In Figs. 4–5 are shown reaction probabilities for $v_f = 1$, 2, and 3 at $E = 0.34$ eV (below Sparks *et al.*[23] sideways peaking energy) and $E = 0.423$ eV (in the range of Sparks *et al.* sideways peaking energy). It is seen that there is no *qualitative* difference between the results. However, at higher energy E and fixed l, the maximum in the $v_f = 2$ results occurs at larger γ. Also, in Figs. 6–7 are shown the reactive probabilities for the energies 0.36 and 0.423 eV as a function of l for several angles γ. Again, there are *no* qualitative differences in the results below the energy at which Sparks *et al.*[23] saw sideways scattering of $HF(v_f = 2)$ and those where such scattering is observed. However, the maximum in the $v_f = 2$ curve for fixed γ occurs at a lower l value for $E = 0.36$ eV than for 0.423 eV. As γ is increased at fixed E, the value of l for which the maximum occurs also decreases. An extremely interesting feature of these results is the fact that the peak height for the $v_f = 2$ curve is independent of l. This strongly suggests that for fixed γ and total energy, increasing l has the effect of "tuning" the system into resonance, decreasing the available kinetic energy in the reaction zone. Similarly, for fixed E and l, increasing γ tunes the system into resonance for $v_f = 2$ again by reducing the available kinetic energy down to the resonance range. At the resonance, the reactive probability has a characteristic value. This suggests that for a *broad range* of collision energy, there will be a range of γ and/or l values which produce resonant reactive scattering into the $v_f = 2$ state of HF. It will be true that for high enough energy E and fixed l, no value of γ produces a high enough potential so as to reduce the effective energy down to the resonant range. However, we do expect that at such an energy, increasing l can again tune the system into resonance. At low enough energy, of course, varying γ and l cannot tune the system into resonance.

In Fig. 8 several primitive probability functions are shown as a function of (total) energy for various γ and l. Again, the curves for $v_f = 2$ give indications of resonance and show the tuning effect alluded to above. It is also seen that the resonant peak broadens and shifts to higher energy as the l value is increased (for fixed γ). However, for $\gamma = 50°$, there does not appear to be a resonance.

Next, in Fig. 16 we note that the *integral* total reactive cross section obtained by the present RIOS method does *not* show a resonance maximum while the CS results of RW do. Although the primitive S matrices in the RIOS do show resonance effects over a certain range of γ and l values for a given energy E, the integration over γ to produce the physical S matrices $S^{v_\nu j_\nu l_\nu}_{J v_\lambda j_\lambda l_\lambda}$, and the sum over l_ν, l_λ to produce the cross section sufficiently broadens these effects and prevents the occurrence of a maximum in the total integral cross section. *Thus, if such a maximum is taken to be a necessary signature of a resonance, then it does not occur in the* RIOS *calculations.* However, it is possible that the occurrence of this maximum in the results of RW is due to their use of a modified MV potential surface.

Continuing this theme for the angular distributions, we emphasize that the effect of varying γ and l to tune the $v_f = 2$ into and out of resonance implies that the resonance effects are not confined to a particular short range of energy. This is also seen clearly by considering Fig. 9 for the angle (γ) averaged reactive probabilities at the three energies 0.36, 0.423, and 0.5 eV. A striking feature is the very flat behavior of the $v_f = 2$ probability as l increases. This occurs because for a given energy and l value, there will be a range of γ values that tune the system into resonance. These resonant contributions are roughly equal for each energy and l value. However, if l becomes too large, then no value

of γ can be found which can produce a large reaction probability (i.e., then the available kinetic energy falls below threshold for the reaction). As a result, the 0.36 eV curve begins falling off sooner with l. *Thus, at the lower energies, the reason that the $v_f = 2$ product is not sideways peaked is because the resonance tuning can only be accomplished with low values of l, or relatively collinear values of γ.* Now Sparks *et al.*[23] have measured the reactive angular distributions as a function of v_f at two energies; specifically, $E_{\text{trans}} = 2$ and 3.17 kcal/mol. They find that at the lower energies, all three products ($v_f = 1$, 2, 3) are backwards peaked ($\theta = \pi$) just like our results for $E_{\text{trans}} = 0.99$, 1.68, and 2.14 kcal/mol ($\equiv 0.31$, 0.34, and 0.36 eV total energy). However, they found that at 3.17 kcal/mol, only $v_f = 1$ and 3 are backwards peaked while the $v_f = 2$ has its maximum at an angle of about 120°.[67] Our results at $E_{\text{tot}} = 0.423$ eV show a secondary maximum at about 70° and the $E_{\text{tot}} = 0.5$ eV results show the maximum scattering at about 60°. However, the present calculations reveal that even at 0.31 eV total energy, one may already detect in Fig. 11 the beginning rise of a sideways peak in the $v_f = 2$ angular distribution. In Figs. 12–13, this is seen to grow even though we are still below Sparks' *et al.*[23] sideways peaking energy. However, in Fig. 15, the energy is high enough so that the range of γ and l values required to tune the resonance are such as to produce the largest scattering in the sideways direction. Finally, we note that the $v_f = 1$ product also appear to show important tuning effects of the variation of the reactive probability with l and γ. Indeed, at the collision energy of 0.5 eV, we predict the $v_f = 1$ product will also be preferentially sideways scattered. This behavior for $v_f = 1$ is a prediction which is yet to be experimentally verified. *The essential point to be made on these results is that this effect of resonant tuning due to variation of the $v_f = 2$ reaction probability with γ and l does not give rise to a resonance in the usual sense* (i.e., *one which is well localized as a function of energy*). *Rather, the effects can in principle be seen (with sufficiently sensitive measurements) over a very broad range of energy. As a result, the usual resonance signatures may be absent.* Of course, at a sufficiently low energy, no variation of γ and l can produce resonance and so there will be a lower limit to the energy at which an effect will occur. It should also be emphasized that if there is some *nonresonant* effect which causes one reaction path to be strongly favored over another for a given range of γ and l values, it can give rise to the same same sort of effect on the angular distributions. All that is required is some mechanism which causes a strong variation in reactivity into a particular state (or states) as l and/or γ change.

Another important feature of the angular distributions for $v_f = 2$ is the presence of oscillations as the energy is increased so that resonance processes make an increased contribution to the scattering. For example, at $E_{\text{tot}} = 0.423$ and 0.5 eV, there is a significant oscillation close to π. Close examination indicates that Sparks' *et al.*[23] results possibly show this behavior also. This is most likely due to interference between resonance and nonresonance contributions to the scattering.

We close this discussion by pointing out that recent calculations by Truhlar and Blais[68] show that quasiclassical trajectories result in backward scattered products independent of the final vibrational state. Also, it was recently mentioned (without giving detailed results)[36] that *all* exact CL calculations done for energies below 5 kcal/mol led to backwards peaked scattering, which is in contradiction to the experimental and present quantal RIOS results. *Thus, we conclude on the basis of the present study and these* CL *results that these experimental results do indeed show quantum effects.*

C. Other quantum effects in the $F + H_2$ system

Although we believe that evidences for resonant effects have been found in the present work, we also feel that the $F + H_2$ system is strongly affected by other quantum phenomena which also cannot be obtained by the quasiclassical method.

In Fig. 18 are presented the branching ratios $\lambda(3, 2)$ and as can be clearly seen, the IOS and CS branching ratios differ very greatly from both the exact CL and IOS CL ones. This finding is reminiscent of what happens in the collinear $F + H_2$ reaction for the energy range $E_{\text{trans}} = [0.01 - 0.08]$ eV [see Fig. 8(a)] but appears to be shifted to higher energies as either l or γ are increased [see Figs. 8(b)–8(f)]. This shifting to higher energies as l and/or γ are increased can be explained as follows. The increase in l reflects the fact that larger l values produce a centrifugal potential whose effect is to decrease the relative translational motion of the system. Thus, the effective kinetic energy is lower and as a result, the $v_f = 2$ state is favored over either the $v_f = 3$ or 1, just as in the low translational energy region of the collinear $F + H_2$. The same type of effect occurs as γ is increased. In this case, the potential energy increases again reducing the available translational energy and producing a dominance of the $v_f = 2$ over either $v_f = 1$ or 3.

The fact that the CL treatment tends to populate the $v_f = 3$ more than does the QM treatment may be connected to the way the final state is discretized in the CL method (i.e., the "boxing" procedure). This discretization is done by assigning any trajectory with final vibrational energy in the vibrational "box" [2.5 $\hbar\omega$, 3.5 $\hbar\omega$] to the $v_f = 3$ state. This procedure, in general, is straightforward so long as the final state is classically easily accessible. However, in limiting cases, where e.g., the vibrational state of interest is almost energetically closed, it may lead to erroneous results. The $v_f = 3$ is not only "almost" closed in the low energy region but also has, in the exit channel, a barrier[66] which affects the $v_f = 3$ population very strongly in the QM treatment, compared to the CL treatment. In this context it should be mentioned that another way of discretizing classical results, i.e., employing classical moments,[61] also failed to yield a vibrational distribution in agreement with QM results.

V. SUMMARY

In this work we have presented numerical results for the reactive $F + H_2$ system which were obtained using

the IOS. In order to get as much insight as possible, results at different stages of the calculation were shown, ranging from the most detailed γ and l-dependent phases, S-matrix elements and probabilities, through angle averaged probabilities and opacities and finally various state-to-state differential cross sections. In the latter case, qualitative agreement with experiment was obtained. In the case of the vibrational branching ratios only a partial fit with experiment was achieved but the disagreement appears to apply not only to the RIOS results but also to the CS results obtained earlier by Redmon and Wyatt. We believe this indicates that these branching ratios display quantum effects. As for the total cross sections, the l-average QM IOS results appear to be accurate since they agree quite well with exact classical results and the evidence is strongly against large quantum effects in this quantity. The l-initial version does not give sufficient accuracy for these cross sections.

We have seen that the IOS *is* capable of correctly describing complicated quantum behavior in systems such as $F + H_2$ and thus provides a theoretical tool with predictive capabilities. Therefore, judging from the results obtained for $F + H_2$ here and in our earlier $H + H_2$ study, it seems that the reactive IOS should be considered as a basic numerical tool for performing reactive dynamics studies. Unlike the close coupling procedure it is a relatively inexpensive method that can be applied to many other atom-diatom systems, and unlike the straightforward classical trajectory method, it can describe quantum effects.

This, however, by no means suggests that the method is fully developed. On the contrary, more research is needed to improve and extend its applicability as well as the efficiency of the numerical aspects. However, we believe the results obtained to date indicate that this direction of research is extremely promising.

ACKNOWLEDGMENTS

The authors express thanks for helpful discussions with and comments by Dr. R. E. Wyatt and Dr. E. F. Hayes. They also thank Dr. Y. T. Lee for sending us information about the experimental results.

[1]V. Khare, D. J. Kouri, and M. Baer, J. Chem. Phys. **71**, 1188 (1979).
[2]J. M. Bowman and K. T. Lee, J. Chem. Phys. **72**, 5071 (1980).
[3]G. D. Barg and G. D. Drolshagen, Chem. Phys. **47**, 209 (1980).
[4]M. Baer, V. Khare, and D. J. Kouri, Chem. Phys. Lett. **68**, 378 (1979).
[5]J. M. Bowman and K. T. Lee, Chem. Phys. Lett. **64**, 29 (1979).
[6]M. Baer, H. R. Mayne, V. Khare, and D. J. Kouri, Chem. Phys. Lett. **72**, 269 (1980).
[7]D. J. Kouri, V. Khare, and M. Baer, J. Chem. Phys. **75**, 1179 (1981).
[8]V. Khare, D. J. Kouri, J. Jellinek, and M. Baer, in *Potential Energy Surfaces and Dynamics Calculations*, edited by D. G. Truhlar (Plenum, New York 1981) pp. 475–493.
[9]M. Baer, in *Advances in Chemical Physics*, edited by I. Prigogine and S. A. Rice (Wiley, New York, 1981).
[10]J. Jellinek, M. Baer, V. Khare, and D. J. Kouri, Chem. Phys. Lett. **75**, 460 (1980).
[11]R. W. Gross and J. F. Bott, *Handbook of Chemical Lasers* (Wiley, New York, 1976).
[12]A. N. Chester, in *High Power Lasers*, edited by E. R. Pike, (Institute of Physics, London, 1967).
[13]Z. B. Alfassi and M. Baer, IEEE J. Quantum Electron. QE-**15**, 240 (1979).
[14]V. I. Igoshin, L. V. Kulatov, and A. I. Nikitin, Sov. J. Quantum. Electron. **3**, 306 (1974).
[15]V. P. Bulatov, V. P. Balakhin, and O. M. Sarkisov, Akad. Nauk. SSSR Div. Chem. Sci. **26**, 1600 (1977).
[16]R. F. Heidner, J. F. Bott, G. E. Gardner, and J. E. Melzer, J. Chem. Phys. **72**, 4815 (1980).
[17]E. Wurzberg and P. L. Houston, J. Chem. Phys. **72**, 4811 (1980).
[18]N. Jonathan, C. M. Melier-Smith, S. Okuda, D. H. Slater, and D. Timlin, Mol. Phys. **22**, 561 (1971).
[19]J. C. Polanyi and K. Woodall, J. Chem. Phys. **57**, 1574 (1972).
[20]R. D. Coombe and G. C. Pimentel, J. Chem. Phys. **59**, 251 (1973).
[21]H. W. Chang and D. W. Setser, J. Chem. Phys. **58**, 2298 (1973).
[22]M. J. Berry, J. Chem. Phys. **59**, 6229 (1973).
[23]R. K. Sparks, C. C. Hayden, K. Shobatake, D. M. Neumark, and Y. T. Lee, in *Horizons of Quantum Chemistry*, edited by K. Fukui and B. Pullman (Reidel, Dordrecht, 1980).
[24]J. B. Anderson, J. Chem. Phys. **52**, 3829 (1970).
[25]J. T. Muckerman, J. Chem. Phys. **54**, 1155 (1971); **56**, 2997 (1972).
[26]R. L. Wilkins, J. Chem. Phys. **57**, 912 (1972).
[27]N. C. Blais and D. G. Truhlar, J. Chem. Phys. **58**, 1090 (1973).
[28]J. C. Polanyi and J. L. Schreiber, Faraday Discuss. Chem. Soc. **62**, 267 (1977).
[29]M. B. Faist and J. T. Muckerman, J. Chem. Phys. **71**, 3450 (1979).
[30]I. Last and M. Baer, J. Chem. Phys. **75**, 288 (1980).
[31]C. F. Bender, P. K. Pearson, S. V. O'Neil, and H. F. Schaefer, J. Chem. Phys. **56**, 4626 (1972).
[32]R. L. Jaffe, K. Morokuma, and T. T. George, J. Chem. Phys. **63**, 3417 (1975).
[33]W. R. Wadt and N. W. Winter, J. Chem. Phys. **67**, 3068 (1977).
[34]S. R. Ungemach, H. F. Schaefer, B. Liu, Faraday Discuss. Chem. Soc. **62**, 330 (1977).
[35]P. Botschwina and W. Mayer, Chem. Phys. **20**, 43 (1977).
[36]J. T. Muckerman, in *Theoretical Chemistry: Advances and Perspectives* 6*A*, edited by H. Eyring and D. H. Henderson (Academic, New York, 1981).
[37]R. L. Jaffe and J. B. Anderson, J. Chem. Phys. **54**, 2224 (1971).
[38]D. F. Feng, E. R. Grant, and J. W. Root, J. Chem. Phys. **64**, 3450 (1976).
[39]A. Komornicki, K. Morokuma, and T. F. George, J. Chem. Phys. **67**, 5012 (1977).
[40]J. N. L. Connor, W. Jakubetz, J. Manz, and J. C. Whitehead, Chem. Phys. **39**, 395 (1979).
[41]S. F. Wu, B. R. Johnson, and R. D. Levine, Mol. Phys **25**, 839 (1973).
[42]G. C. Schatz, J. M. Bowman, and A. Kuppermann, J. Chem. Phys. **56**, 1024 (1973); **63**, 674 (1975).
[43]J. N. L. Connor, W. Jakubetz, and J. Manz, Mol. Phys. **29**, 347 (1975).
[44]J. T. Adams, R. L. Smith, and E. F. Hayes, J. Chem. Phys. **61**, 2193 (1974); see also E. F. Hayes and R. B. Walker, J. Phys. Chem. **86**, 85 (1982).
[45]S. L. Latham, J. F. McNutt, R. E. Wyatt, and M. J. Redmon, J. Chem. Phys. **69**, 3746 (1978).
[46]J. S. Hutchinson and R. E. Wyatt, J. Chem. Phys. **70**,

3509 (1979).
[47]M. J. Redmon and R. E. Wyatt, Chem. Phys. Lett **63**, 209 (1979); R. E. Wyatt, J. F. McNutt, and M. J. Redmon, Ber. Bunsenges. Phys. Chem. (in press).
[48]M. Baer, J. Chem. Phys. **62**, 4545 (1975).
[49]A. B. Shaul, R. D. Levine, and R. B. Bernstein, J. Chem. Phys. **57**, 5427 (1972).
[50]J. N. L. Connor, W. Jakubetz, and J. Manz, Chem. Phys. **17**, 451 (1976).
[51]G. Venzl and S. F. Fischer, J. Chem. Phys. **71**, 4175 (1979).
[52]I. H. Zimmerman, M. Baer, and T. F. George, J. Chem. Phys. **71**, 4132 (1979).
[53]A. Kuppermann, G. C. Schatz, and M. Baer, J. Chem. Phys. **65**, 4596 (1976).
[54]A. B. Elkowitz and R. E. Wyatt, J. Chem. Phys. **63**, 702 (1975).
[55]R. B. Walker, J. C. Light, and A. Altenberger-Siczek, J. Chem. Phys. **67**, 1166 (1976).
[56]M. E. Rose, *Elementary Theory of Angular Momentum* (Wiley, New York, 1952).
[57]A. M. Arthurs and A. Dalgarno, Proc. R. Soc. London Ser. A **256**, 540 (1960).
[58]The original l-labeled version of the CS for nonreactive scattering is P. McGuire and D. J. Kouri, J. Chem. Phys. **60**, 2488 (1974). The J-labeled CS was developed independently by R. T Pack, J. Chem. Phys. **60**, 633 (1974). Additional work on l-labeling includes that of D. Secrest, J. Chem. Phys. **62**, 710 (1975); Y. Shimoni and D. J. Kouri, *ibid.* **65**, 3372 and 3958 (1976) and **66**, 675 and 2841 (1977); D. G. Truhlar, R. E. Poling, and M. A. Brandt, *ibid.* **64**, 826 (1976); G. A. Parker and R. T. Pack, *ibid.* **66**, 2850 (1977); D. J. Kouri and Y. Shimoni, *ibid* **67**, 86 (1977); R. Goldflam and D. J. Kouri, *ibid.* **66**, 542 (1977); V. Khare, *ibid.* **67**, 3897 (1977); L. Monchick, *ibid.***67**, 4626 (1977); D. J. Kouri, R. Goldflam, and Y. Shimoni, *ibid.* **67**, 4534 (1977); D. E. Fitz. Chem. Phys. **24**, 133 (1977); V. Khare, D. J. Kouri, and R. T Pack, J. Chem. Phys. **69**, 4419 (1978); D. E. Fitz, Chem. Phys. Lett. **55**, 202 (1978); R. Schinke and P. McGuire, Chem. Phys. **28**, 129 (1978); L. Monchick and D. J. Kouri, J. Chem. Phys. **69**, 3262 (1978); D. A. Coombe and R. F. Snider, *ibid.* **71**, 4284 (1979); S. Stolte and J. Reuss, in *Atom-Molecule Collision Theory: A Guide for the Experimentalist*, edited by R. B. Bernstein (Plenum, New York, 1979); D. J. Kouri, in *Atom-Molecule Collision Theory: A Guide for the Experimentalist*, edited by R. B. Bernstein (Plenum, New York, 1979).
[59]The most recent work has shown that the average-l choice of $\bar{l}$ in the CS (and IOS), first suggested in unpublished notes by D. Secrest, is the best choice suggested to date. This has been fully explicated in V. Khare, D. J. Kouri, and D. K. Hoffman, J. Chem. Phys. **74**, 2275 (1981); V. Khare, D. E. Fitz, and D. J. Kouri, *ibid.* **73**, 2802 and 4148 (1980); and V. Khare and D. J. Kouri, Chem. Phys. Lett. **80**, 262 (1981). Finally, the first demonstration that j_z is approximated preserved in exact CC results for molecular scattering (provided the axis is taken to be a generalized apse) was given by V. Khare, D. J. Kouri, and D. K. Hoffman, J. Chem. Phys. **74**, 2656 (1981).
[60]J. Jellinek and M. Baer, J. Chem. Phys. (in press).
[61]J. Jellinek and M. Baer, Chem. Phys. Lett. **82**, 162 (1981).
[62]J. Jellinek and M. Baer, (to be published).
[63]R. Goldflam, S. Green, and D. J. Kouri, J. Chem. Phys. 67 **67**, 4149 and 5661 (1977).
[64]J. Jellinek, M. Baer, and D. J. Kouri (to be published).
[65]G. Breit and E. P. Wigner, Phys. Rev. **49**, 519 (1936).
[66]E. Pollak, J. Chem. Phys. **74**, 5586 (1981).
[67]Y. T. Lee (private communication).
[68]D. G. Truhlar and N. C. Blais (to be published).